Two-Conductor Ports Enabling Broadband Operation of Substrateless Microscale Silicon Waveguides

Daniel Headland, *Member, IEEE*, Daniel C. Gallego, and Guillermo Carpintero, *Senior Member, IEEE*

***Abstract*—We extend the operation bandwidth of substrateless all-silicon waveguides beyond the single-mode region. This requires a suitably broadband port-access scheme, as well as careful management of undesired higher order modes. It is found that a length of two-conductor waveguide serves both purposes. In this way, we experimentally demonstrate broadband power transfer between dielectric waveguides and numerically investigate suppression of higher order modes. This 3-D solid-metal two-conductor waveguide shows promise as a package-external terahertz port, to address the 40% relative-bandwidth bottleneck that is currently imposed by hollow metallic waveguides. This represents a step toward efficient handheld terahertz systems that fully exploit the broad available spectrum.**

***Index Terms*—Broadband, integration, mm-wave, photonics, port, silicon, substrateless, waveguide, terahertz.**

I. Introduction

WAVEGUIDES are generally operated in the single-mode region to avoid the copropagation of higher order modes, which can compromise signal integrity. However, single-mode operation reduces achievable bandwidth, e.g., to 40% for single-conductor hollow metallic waveguides [1]. This is a disadvantage for terahertz systems, as many attractive envisaged applications such as spectroscopy [2] and frequency-agile communications [3] demand broad spectrum. There do exist two- and three-conductor waveguides that are single-mode in broadband (i.e., greater than an octave), such as coaxial cables [4] and coplanar waveguides [5]. However, the conduction loss is unacceptably high, with coplanar waveguides in particular having 30 dB/cm at 400–500 GHz [5]. It is therefore wise to deploy as little conductive line as possible.

Substrateless terahertz silicon dielectric waveguides are showing promise as low-loss interconnect, albeit generally restricted to at most 40% bandwidth in order to avoid undesired higher order modes [6]. That said, it has previously been shown that single-mode operation in the multimode region of the dielectric rod waveguide, whilst avoiding adverse effects of higher order modes, is potentially viable [7], [8]. However, those demonstrations made use of single-mode hollow metallic waveguides to excite the dielectric waveguide, and so the span available to the overall configuration remains bottlenecked at 40% by the launching port. To increase this bandwidth, here we explore practical considerations toward operation of microscale substrateless silicon dielectric waveguides over a continuous unsegmented span that begins at the single-mode region and extends into the multimode region. To support this aim, we have identified three critical necessary requirements. The first is accurate positioning and alignment of coupler structures in order to maximize the yield of the desired fundamental mode. The second is mode-filtering functionality, to remove any residual power in undesired higher order modes. The final requirement is an external access port to convey the entire broad spectral bandwidth to other devices and systems, in contrast to the aforementioned 40% bottleneck that arises when hollow metallic waveguides are used for this purpose.

For substrateless waveguides, accurate positioning and alignment benefits greatly from the monolithic integration of a surrounding frame to enable handling without physically touching the exposed waveguide core [6]. The waveguide can be structurally anchored to the frame via a periodic through-hole lattice that acts as effective medium [9], although it is noted that this periodicity carries potential for undesired stopbands due to Bragg effects as operation frequency is increased [10]. Fortunately, however, in this work we find no evidence of such Bragg effects over a broad ∼4:1 range that begins with the onset of the fundamental guided mode.

If we accept that, in reality, we cannot wholly avoid the possibility of exciting higher order modes, then this motivates the development of mode-filters to remove them from the waveguide. To this end, we may incorporate a short section of two-conductor, single-mode metallic waveguide that only allows for the transfer of the fundamental mode between two multimode silicon waveguides. The result is a broadband interposer, and

Manuscript received 6 February 2024; revised 17 April 2024; accepted 23 May 2024. Date of publication 30 May 2024; date of current version 5 July 2024. The work of Daniel Headland was supported by the CONEX-Plus programme funded by Universidad Carlos III de Madrid and the European Union's Horizon 2020 research and innovation programme Marie Sklodowska-Curie under Grant 801538. This work was supported by the Research Executive Agency (REA) through TERAmeasure project under Grant 862788, in part by the Smart Networks and Services Joint Undertaking (SNS JU) through the European Union's Horizon Europe research and innovation programme under Grant 101096949 (TERA6G project), and in part by the APC: Universidad Carlos III de Madrid (Agreement CRUE-Madroño 2024). *(Corresponding author: Daniel Headland.)*

Daniel Headland is with the Optoelectronics and Laser Technology Group, Department of Electronics Technology, Universidad Carlos III de Madrid, 28911 Madrid, Spain (e-mail: dheadlan@ing.uc3m.es).

Daniel C. Gallego is with the LeapWave Technologies, 28919 Madrid, Spain.

Guillermo Carpintero is with the Optoelectronics and Laser Technology Group, Department of Electronics Technology, Universidad Carlos III de Madrid, 28911 Madrid, Spain, and also with the LeapWave Technologies, 28919 Madrid, Spain.

This article has supplementary material provided by the authors and color versions of one or more figures available at https://doi.org/10.1109/TTHZ.2024.3407686.

Digital Object Identifier 10.1109/TTHZ.2024.3407686

although it exhibits Ohmic loss, this will be minimized if only a short length is used.

We employ a double-ridged waveguide, which is closely related to a planar slotline, for which broadband interfaces to dielectric waveguides have previously been demonstrated [11], [12], [13], [14]. Here, we implement an interposer by terminating a short length of the two-conductor waveguide with such an interface at both ends, and broadband transfer of power is experimentally verified. It is also noted that this manner of two-conductor waveguide is closely related to two-wire waveguides, in that it is a symmetrical two-conductor linear waveguide with two-dimensional cross-sectional confinement, and also to parallel-plate waveguides, in that power is confined within a narrow gap between two solid-metal conductors. Both of these waveguides have been studied extensively in the terahertz range [15], [16], [17], [18], but must be excited using cumbersome free-space beams due to a lack of viable interposers. The dielectric-waveguide interface that we present here is a solution to address this lack. In other words, although the two-conductor waveguide is employed as an interposer for silicon dielectric waveguides in the current work, one could also equally view the dielectric waveguide as an interposer for the two-conductor waveguide, rendering the latter amenable to compact handheld devices.

The two-conductor interposer is composed of solid metal, making it sufficiently robust to be exposed as an interface to the external world. The same cannot be said of substrateless microscale silicon components, especially considering that the most common form of coupler is a tapered spike [6], which is vulnerable to breakage. Not only that, this coupler also poses safety risks, as it is sufficiently sharp to cause puncture wounds. Furthermore, near-field interfaces between dielectric waveguides tend to be strongly frequency-dependent [19], [20], and in view of these facts, a viable broadband all-silicon external access port seems unlikely. To address this lack, the double-ridged slot waveguide shows promise as a broadband analog of robust, detachable 40%-bandwidth hollow metallic waveguide access ports. Both of these waveguides are single-mode, and so power that appears in the guide can be expressed straightforwardly as a single complex amplitude coefficient, as opposed to a detailed mode composition as in overmoded waveguides, or a complete 2-D field-aperture distribution for free-space interfaces. Thus, the two-conductor waveguide is promising as an external access-port interface for future broadband packaged terahertz systems that are internally interconnected with low-loss overmoded substrateless silicon waveguides.

II. Design and Simulation

A. Few-Mode Silicon waveguide

We employ a substrateless all-intrinsic-silicon structure that surrounds an unclad core with a protective frame [9], as shown in Fig. 1(a). The waveguide core is anchored at both ends with a periodic through-hole lattice that guided waves experience as a low-index effective medium that is close to the air cladding. Substrateless all-intrinsic-silicon effective-medium-clad waveguides of this sort are known to exhibit low propagation loss of

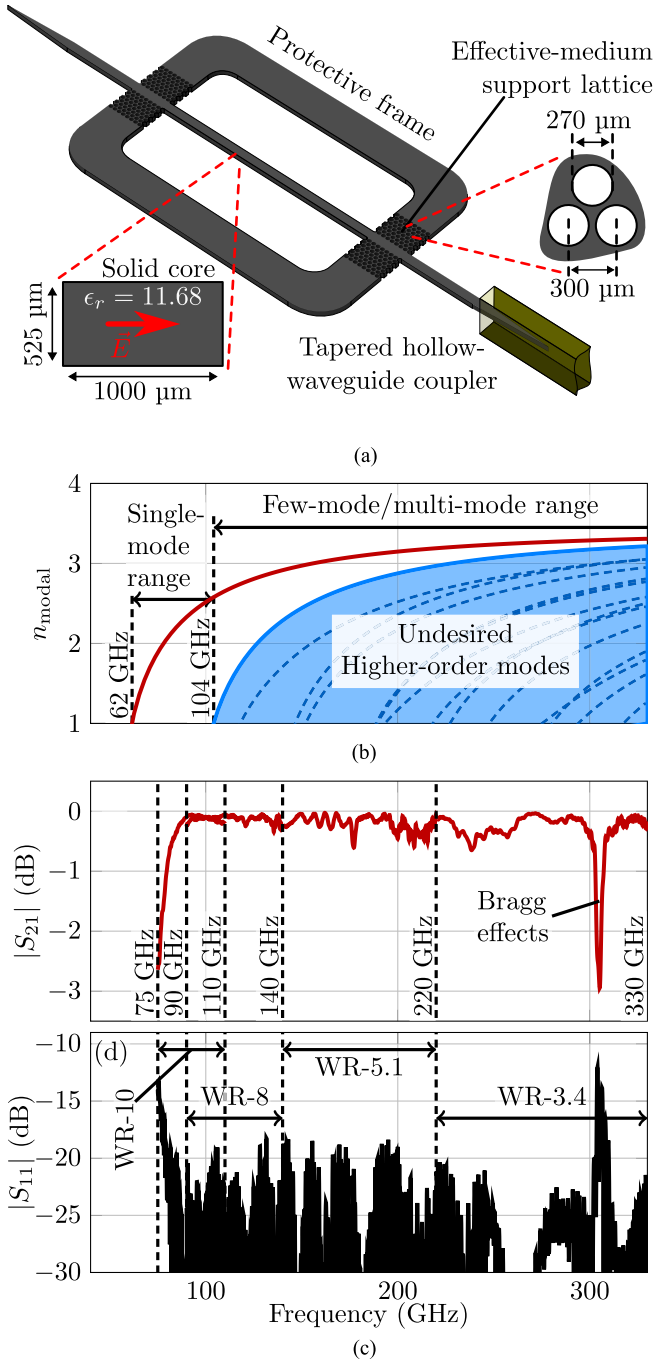

Fig. 1. Design and simulation of an unclad microphotonic waveguide, showing (a) illustration of the device platform, with hollow-waveguide interface shown at one of the terminations, (b) modal analysis in broadband, and (c),(d) simulated response using four different hollow-metallic waveguides bands, where each corresponds to a distinct single-mode range that demands specific inner-conductor dimensions.

<0.1 dB/cm in the frequency range of interest [6]. Modal analysis using Marcatili's method [6], [21], [22] is given in Fig. 1(b), showing that the single-mode range of our structure, i.e., the span over which only a single mode has $n_{\text{modal}} > 1$, is 62–104 GHz. This means that, in this range, only this fundamental mode may propagate indefinitely without progressive radiation to the surrounding space, and hence is nonleaky. Below this range the waveguide continuously radiates power to free-space as in a

uniform leaky-wave antenna [23], and this unguided propagation defines the lower limit of waveguide operation, analogous to a hollow metallic waveguide's cutoff. Above the single-mode range, higher order modes also propagate without leakage.

Current mm-wave and terahertz-range convention is to excite dielectric waveguides by tapering the termination to a spike that is then inserted into the inner volume of a single-mode hollow metallic waveguide [6], [9], [12], [24], [25], [26], and it is noted that a single spike of fixed geometry can access several hollow-waveguide bands of different inner-conductor dimensions [7], [8], [12]. Thus, broadband numerical investigation of the structure illustrated in Fig. 1(a) requires a series of full-wave simulations, for which we deploy the commercial software package CST Studio Suite, and the results are shown in Fig. 1(c) and1(d). High transmission efficiency and low return loss are observed well into the silicon waveguide's multimode region, and so the impact of higher order modes is negligible. The only spectral feature of note is a narrow dip in transmission just above 300 GHz, which is ascribed to Bragg effects caused by the periodicity of the effective-medium support [10]. Thus, the upper-bound of operation bandwidth spans from the onset of the transmission bandwidth at 75 GHz up until the Bragg effects above 300 GHz, for a ∼4:1 range. Note that this excludes the lower-end of the silicon waveguide's single-mode region, i.e., from 62 to 75 GHz, as strong delocalization of guided waves at low frequencies increases coupling loss.

B. Broadband Interposer and Mode-Filter

A microscale two-conductor ridge slot waveguide is devised. Separation between conductors is set to a half-wave at the chosen upper-frequency limit of 300 GHz in order to inhibit higher order modes [27], whilst avoiding excessive Ohmic loss and physical clearance issues that would arise from a narrow gap. The thickness of the conductor is likewise 500 μm in order to achieve close confinement in the vicinity of the rod whilst maintaining sufficient bulk metal for a robust and inflexible structure. We terminate both ends of a short length of this double-ridge waveguide with a Vivaldi antenna, realizing the interposer shown in Fig. 2(a). Closely related structures have previously been demonstrated, albeit with the antenna serving as free-space interface [28], [29], [30]. In contrast, here the Vivaldi antenna serves a broadband interface to a dielectric waveguide by inserting the waveguide's tapered-spike termination into the throat of the Vivaldi antenna [11], [12], [13], [14], [31], [32]. Both constituents mutually compensate for the longitudinal variation of field hand-off point [12], achieving broadband transfer of power, although it is important to note that these cited works have all described planar transitions, which serve solely for on-chip, or on-circuitboard connections. In contrast, here we consider a robust, freestanding solid metal structure, the performance of which we investigate using full-wave simulations. The results in Fig. 2(b) show 66% overall efficiency, or 81% for a single coupler, as well as >4:1 3-dB transmission bandwidth for the fundamental mode. Additional simulations shown in the supplementary information that accompanies this manuscript confirm that our chosen double-ridge waveguide parameters are optimal.

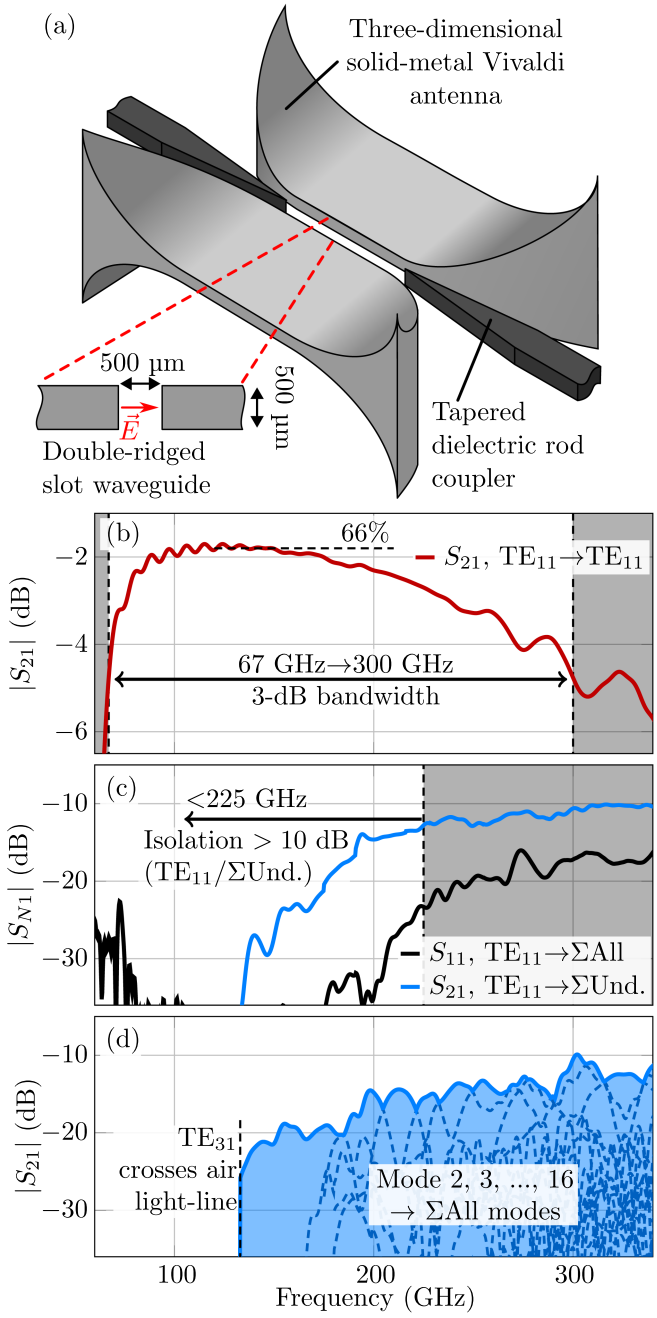

Fig. 2. Broadband metal interposer and mode-filter for silicon dielectric rod waveguides, showing (a) illustration of the structure, (b) simulated transmission of the desired, fundamental mode, (c) undesired output in response to excitation with the desired, fundamental mode, where the sum of output power has been taken across all modes indicated, and (d) rejection of higher order modes, where each individual mode is excited, and the transmitted power is summed across all modes. Power in leaky modes (i.e., below the air light-line) is disregarded.

Low reflection is observed in Fig. 2(c), and the aggregate yield of undesired modes is −10 dB lower than that of the fundamental for frequencies below 225 GHz. We consider the intersection of the 3-dB bandwidth with this range to be the interposer's operation bandwidth, which is >3:1, i.e., from 67 to 225 GHz. It is noted that prior related overmoded dielectric waveguide work [7], [8], [12], [13], [14] did not quantitatively consider mode composition in this way, and hence lacked a critical

comparative measure of the yield of the desired fundamental mode.

It is possible that a higher order mode of the silicon waveguide will be incident upon the interposer, and so it is prudent to repeat the simulation for each such mode. In each case, the total aggregate power conveyed to all modes of the receiving waveguide is shown in Fig. 2(d). The maximum aggregate transmission of these higher order modes is below 3.6% over the aforementioned >3:1 range, and so we conclude that the two-conductor section serves as an effective mode filter in addition to being an interposer for silicon waveguides.

III. Experimental Proof of Concept

Two silicon waveguide samples are fabricated using deep reactive ion etching, and the interposer is computer numerical control (CNC)-machined from aluminum along with custom packages. The package suspends the waveguide core over a trench, and offers interlocking structures for precise alignment to standard hollow-waveguide flanges [24], [25], [26], [33], as shown in Fig. 3(a)–(c). The silicon part is placed into a shallow depression that corresponds to the outer edge of the protective frame, with a 50-μm margin on either side to account for tolerances. We have found it necessary to perform manual adjustment of position using handheld tweezers in order to compensate for the aforementioned margin. Future iterations of this package design must therefore incorporate a repeatable fine-adjustment mechanism via contact with the frame.

Experiments are performed using a vector network analyzer equipped with frequency extension modules that offer hollow-waveguide interfaces. In order to characterize the interposer's operation bandwidth, we perform separate experiments using WR-10 and WR-5.1 extension modules, where the insertion depth of the tapered spike is set with 3D-printed plastic spacers in each case. Straight hollow metallic waveguides are attached prior to installation in the instrumentation system, as this lowers breakage risk during assembly, although in the case of the WR-5.1 band, only one side may be outfitted in this way due to limited available components.

Experimental results are given in Fig. 3(d) and 3(e), showing broadband transmission and low reflection. Neither individual measurement of the interposer encounters a 3-dB limit, and if the increased coupling loss at WR-5.1 is taken into account, then this statement can also be made for the two bands collectively. Speaking of coupling loss, it is noted that both bands show lower efficiency than in simulation at the lower-frequency edge, possibly due to the influence of the solid-metal flange. Away from this edge, in the WR-10 band, the interposer exhibits ~ -1.5 dB peak efficiency, which is less than 1 dB in excess of that of a single silicon waveguide. In the WR-5.1 band, peak efficiency falls to ~ -3.5 dB, which is $\sim$2.5 dB in excess of the loss experienced by the straight waveguides, corresponding to 75% efficiency for a single coupler. The overall transmission is therefore $\sim$0.5 dB lower than expected, which may be partly due to surface roughness on the CNC-machined surface of the double-ridge waveguide, or to lower conductivity than in simulation. Another possible culprit is minor misalignment, to which we also ascribe the $\sim$1 dB variation that is observed in the single WR-5.1-band silicon-waveguide measurements shown in Fig. 3(d). Cross-comparison with purposefully misaligned full-wave simulations (not shown) indicate that $\sim 0.08^\circ$ rotation of the silicon sample would cause comparable variation, which we believe is entirely possible in practice due to the tolerances of the package. The variation of the interposer is higher, at $\sim$1.5 dB, as each individual silicon waveguide is an independent source of this misalignment error. Phenomenologically, this misalignment excites higher order modes that are ultimately rejected by the receiving hollow-metallic waveguide, leading to interference fringes and hence variation. It is therefore a critical issue to address in order to effective manage higher-order modes.

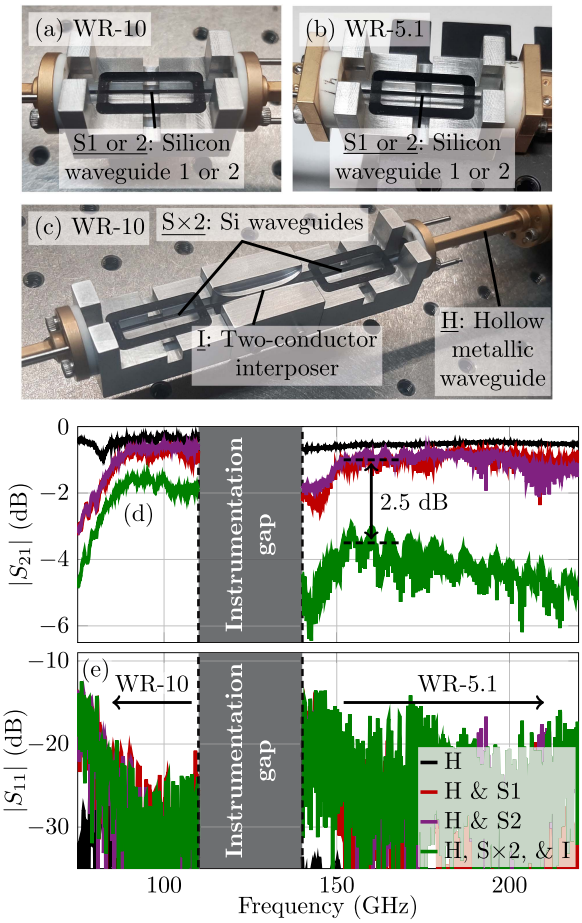

Fig. 3. Experimental characterization, showing (a) and (b) packaged single silicon waveguide undergoing characterization in WR-10 and WR-5.1 bands, (c) interposer characterization in WR-10 band, and (d) and (e) measured magnitude spectra extracted directly from the VNA, with no further processing. The shorthand notation in the legend denotes in-series waveguide combinations, e.g., "H & S1" corresponds to the hollow metallic waveguide(s) together with a silicon waveguide, and so the loss of S1 is referenced to that of H, i.e., the hollow waveguide in isolation.

IV. Conclusion and Further Work

Substrateless silicon waveguides have broadband potential, but exploitation thereof demands suitably broadband port-access, for which we have shown that an interposer composed of a two-conductor waveguide terminated with Vivaldi-antenna flares can serve well. The restriction that we aim to alleviate is readily observable in Fig. 1(c) and 1(d), and

in 3(d) and 3(e), which are segmented into 40% bandwidth allocations due to the use of hollow metallic waveguides. In contrast, Fig. 2(b)–2(c) do not incorporate a hollow metallic waveguide, and so they show continuous, unsegmented spectra. Experimental and numerical investigation of the two-conductor interposer show broadband transmission in a >3:1 range, as well as strong selectivity for the desired fundamental mode. The achieved coupling efficiency is commensurate with that of related planar broadband dielectric waveguide couplers [13].

Future iterations of the package design will incorporate adjustment mechanisms, such as screws for fine manual alignment, for which the protective frame is key, as direct contact with the core would disturb the fields therein. We also believe that, with careful refinements to the design of the Vivaldi antenna and tapered silicon spike, the operation bandwidth may be increased to the ∼4:1 Bragg-limited span. Operation may also be adapted to beyond 1 THz by physically-scaling the silicon [34] and metal components [30], although this would incur markedly increased Ohmic loss.

IV. Acknowledgment

The authors would like to thank VMicro S. A. S. for silicon fabrication, Mr Jose Antonio Campo Santos for CNC-machining, and Dr Muhsin Ali for 3D-printing assistance.

References

[1] N. Ridler and R. Ginleyt, "A review of the IEEE 1785 standards for rectangular waveguides above 110 GHz," in *Proc. 89th ARFTG Microw. Meas. Conf.*, 2017, pp. 1–4.

[2] P. U. Jepsen, D. G. Cooke, and M. Koch, "Terahertz spectroscopy and imaging–modern techniques and applications," *Laser Photon. Rev.*, vol. 5, no. 1, pp. 124–166, 2011.

[3] T. Nagatsuma, G. Ducournau, and C. C. Renaud, "Advances in terahertz communications accelerated by photonics," *Nat. Photon.*, vol. 10, no. 6, pp. 371–379, 2016.

[4] Y.-S. Lee and T. Roberts, "Accuracy study on the newly introduced Anritsu W1-connector calibration and verification kit," in *Proc. 62nd ARFTG Microw. Meas.*, 2003, pp. 109–118.

[5] L. Cao, A.-S. Grimault-Jacquin, N. Zerounian, and F. Aniel, "Design and VNA-measurement of coplanar waveguide (CPW) on benzocyclobutene (BCB) at THz frequencies," *Infrared Phys. Technol.*, vol. 63, pp. 157–164, 2014.

[6] D. Headland, M. Fujita, G. Carpintero, T. Nagatsuma, and W. Withayachumnankul, "Terahertz integration platforms using substrateless all-silicon microstructures," *APL Photon.*, vol. 8, no. 9, 2023, Art. no. 091101.

[7] A. A. Generalov, J. A. Haimakainen, D. V. Lioubtchenko, and A. V. Räisänen, "Wide band mm-and sub-mm-wave dielectric rod waveguide antenna," *IEEE Trans. Terahertz Sci. Technol.*, vol. 4, no. 5, pp. 568–574, Sep. 2014.

[8] M. Ali et al., "Terahertz band data communications using dielectric rod waveguide," in *Proc. OFC*, 2022, pp. W1H–5.

[9] D. Headland, W. Withayachumnankul, X. Yu, M. Fujita, and T. Nagatsuma, "Unclad microphotonics for terahertz waveguides and systems," *J. Lightw. Technol.*, vol. 38, no. 24, pp. 6853–6862, Dec. 2020.

[10] D. Headland, M. Fujita, and T. Nagatsuma, "Bragg-mirror suppression for enhanced bandwidth in terahertz photonic crystal waveguides," *IEEE J. Sel. Topics Quantum Electron.*, vol. 26, no. 2, Mar./Apr. 2020, Art. no. 4900109.

[11] A. Rivera-Lavado et al., "Contactless RF probe interconnect technology enabling broadband testing to the terahertz range," *IEEE Trans. Terahertz Sci. Technol.*, vol. 13, no. 1, pp. 34–43, Jan. 2023.

[12] M. Ali et al., "A novel broadband port-access scheme to interface several waveguide bands to a single Schottky barrier diode detector," in *Proc. 48th Int. Conf. Infrared, Millimeter, Terahertz Waves*, 2023.

[13] S. Iwamatsu et al., "Ultra-wideband multi-octave planar interconnect for multi-band THz communications," *J. Infrared. Millim. Terahertz Waves*, vol. 44, pp. 532–550, 2023.

[14] S. Iwamatsu et al., "Terahertz photodiode integration with multi-octave-bandwidth dielectric rod waveguide probe," *Opt. Lett.*, vol. 48, no. 23, pp. 6275–6278, 2023.

[15] R. Mendis and D. M. Mittleman, "Comparison of the lowest-order transverse-electric (TE_1) and transverse-magnetic (TEM) modes of the parallel-plate waveguide for terahertz pulse applications," *Opt. Exp.*, vol. 17, no. 17, pp. 14839–14850, 2009.

[16] M. Mbonye, R. Mendis, and D. M. Mittleman, "A terahertz two-wire waveguide with low bending loss," *Appl. Phys. Lett.*, vol. 95, no. 23, 2009, Art. no. 233506.

[17] T. Furuya et al., "Terahertz generation in a thin GaAs slab in a tapered parallel plate waveguide by femtosecond laser excitation at 1560 nm," *Japanese J. Appl. Phys.*, vol. 60, no. 7, 2021, Art. no. 072009.

[18] G. Balistreri et al., "Time-domain integration of broadband terahertz pulses in a tapered two-wire waveguide," *Laser Photon. Rev.*, vol. 15, no. 8, 2021, Art. no. 2100051.

[19] J. P. Pousi, S. Dudorov, D. Lioubtchenko, and A. Räisänen, "Frequency selective coupler for W band based on power transfer in dielectric rod waveguides," in *Proc. IEEE 4th Eur. Conf. Antennas Propag.*, 2010, pp. 1–4.

[20] D. Headland, X. Yu, M. Fujita, and T. Nagatsuma, "Near-field out-of-plane coupling between terahertz photonic crystal waveguides," *Optica*, vol. 6, no. 8, pp. 1002–1011, 2019.

[21] E. A. Marcatili, "Dielectric rectangular waveguide and directional coupler for integrated optics," *Bell Syst. Tech. J.*, vol. 48, no. 7, pp. 2071–2102, 1969.

[22] W. J. Westerveld, S. M. Leinders, K. W. van Dongen, H. P. Urbach, and M. Yousefi, "Extension of Marcatili's analytical approach for rectangular silicon optical waveguides," *J. Lightw. Technol.*, vol. 30, no. 14, pp. 2388–2401, Jul. 2012.

[23] D. Headland, Y. Monnai, D. Abbott, C. Fumeaux, and W. Withayachumnankul, "Tutorial: Terahertz beamforming, from concepts to realizations," *APL Photon.*, vol. 3, no. 5, 2018, Art. no. 051101.

[24] A. Malekabadi, S. A. Charlebois, D. Deslandes, and F. Boone, "High-resistivity silicon dielectric ribbon waveguide for single-mode low-loss propagation at F/G-bands," *IEEE Trans. Terahertz Sci. Technol.*, vol. 4, no. 4, pp. 447–453, Jul. 2014.

[25] S. A. Hosseini Farahabadi et al., "Sub-terahertz silicon-based on-chip absorption spectroscopy using thin-film model for biological applications," *Sci. Rep.*, vol. 12, no. 1, 2022, Art. no. 17747.

[26] D. Headland et al., "Broadband mm-wave sealed-volume liquid bio-sensor exploiting tailored delocalization of modal fields in a micro-scale silicon waveguide," in *Proc. 48th Int. Conf. Infrared, Millimeter, Terahertz Waves*, 2023.

[27] J.-W. Sheen and Y.-D. Lin, "Propagation characteristics of the slotline first higher order mode," *IEEE Trans. Microw. Theory Tech.*, vol. 46, no. 11, pp. 1774–1781, Nov. 1998.

[28] R. Peretti, F. Braud, E. Peytavit, E. Dubois, and J.-F. Lampin, "Broadband terahertz light–matter interaction enhancement for precise spectroscopy of thin films and micro-samples," *Photonics*, vol. 5, no. 2, 2018, Art. no. 11.

[29] U. Senica et al., "An antipodal vivaldi antenna for improved far-field properties and polarization manipulation of broadband terahertz quantum cascade lasers," *Appl. Phys. Lett.*, vol. 116, no. 16, 2020, Art. no. 161105.

[30] D. Rohrbach, B. J. Kang, E. Zyaee, and T. Feurer, "Wideband dispersion-free THz waveguide platform," *Sci. Rep.*, vol. 13, no. 1, 2023, Art. no. 15228.

[31] J. Richter, Y. Yazici, C. Ziegler, and L.-P. Schmidt, "A broadband transition between dielectric and planar waveguides at millimeterwave frequencies," in *Proc. IEEE 33rd Eur. Microwave Conf. Proc.*, 2003, pp. 947–950.

[32] I. Ocket, M. Cauwe, and B. Nauwelaers, "Millimeter wave planar transition from plastic rectangular waveguide to 1 mm coax," in *Proc. IEEE MTT-S Int. Microw. Symp.*, 2016.

[33] S. M. Hanham, M. M. Ahmad, S. Lucyszyn, and N. Klein, "LED-switchable high-Q packaged THz microbeam resonators," *IEEE Trans. Terahertz Sci. Technol.*, vol. 7, no. 2, pp. 199–208, Mar. 2017.

[34] R. Koala et al., "Ultra-low-loss and broadband all-silicon dielectric waveguides for WR-1 band (0.75–1.1 THz) modules," *Photon.*, vol. 9, no. 8, 2022, Art. no. 515.